

# JGR Atmospheres

## RESEARCH ARTICLE

10.1029/2020JD034242

### Key Points:

- Both PS\_BVOC and Model of Emissions of Gases and Aerosols from Nature schemes capture reasonable spatial patterns of the global isoprene emissions
- Differences in schemes are the main driver of uncertainties in isoprene trends
- Differences in meteorological forcings dominate the uncertainties in the interannual variability of isoprene emissions

### Supporting Information:

Supporting Information may be found in the online version of this article.

### Correspondence to:

X. Yue,  
[yuexu@nuist.edu.cn](mailto:yuexu@nuist.edu.cn)

### Citation:

Cao, Y., Yue, X., Lei, Y., Zhou, H., Liao, H., Song, Y., et al. (2021). Identifying the drivers of modeling uncertainties in isoprene emissions: Schemes versus meteorological forcings. *Journal of Geophysical Research: Atmospheres*, 126, e2020JD034242. <https://doi.org/10.1029/2020JD034242>

Received 12 NOV 2020

Accepted 25 AUG 2021

### Author Contributions:

**Conceptualization:** Xu Yue

**Data curation:** Yang Cao, Yadong Lei, Hao Zhou, Jianhui Bai, Lei Chen, Jia Zhu, Yimian Ma, Chenguang Tian

**Formal analysis:** Yang Cao

**Investigation:** Hong Liao, Jianhui Bai

**Methodology:** Yu Song

**Supervision:** Xu Yue







**Validation:** Yadong Lei, Yang Yang

**Visualization:** Hao Zhou

**Writing – original draft:** Yang Cao

**Writing – review & editing:** Xu Yue, Hong Liao, Yu Song

## Identifying the Drivers of Modeling Uncertainties in Isoprene Emissions: Schemes Versus Meteorological Forcings

Yang Cao<sup>1,2</sup> , Xu Yue<sup>3</sup> , Yadong Lei<sup>1,2</sup>, Hao Zhou<sup>1,2</sup>, Hong Liao<sup>3</sup> , Yu Song<sup>4</sup> , Jianhui Bai<sup>5</sup>, Yang Yang<sup>3</sup> , Lei Chen<sup>3</sup> , Jia Zhu<sup>3</sup> , Yimian Ma<sup>1,2</sup>, and Chenguang Tian<sup>1,2</sup>

<sup>1</sup>Climate Change Research Center, Institute of Atmospheric Physics (IAP), Chinese Academy of Sciences (CAS), Beijing, China, <sup>2</sup>University of Chinese Academy of Sciences, Beijing, China, <sup>3</sup>Jiangsu Key Laboratory of Atmospheric Environment Monitoring and Pollution Control, Collaborative Innovation Center of Atmospheric Environment and Equipment Technology, School of Environmental Science and Engineering, Nanjing University of Information Science & Technology (NUIST), Nanjing, China, <sup>4</sup>State Key Joint Laboratory of Environmental Simulation and Pollution Control, Department of Environmental Science, Peking University, Beijing, China, <sup>5</sup>Key Laboratory for Middle Atmosphere and Global Environment Observation (LAGEO), IAP, CAS, Beijing, China

**Abstract** Isoprene dominates global biogenic volatile organic compounds and has significant impacts on atmospheric chemistry. Global simulations of isoprene emissions show large uncertainties in both the trend and interannual variability. Here, we explored the uncertainties of simulated isoprene emissions during 1982–2015 using the Yale Interactive terrestrial Biosphere model, which is implemented with two emission schemes (PS\_BVOC and Model of Emissions of Gases and Aerosols from Nature [MEGAN]) and driven by two long-term reanalysis meteorology (WFDEI and Modern-Era Retrospective Analysis for Research and Applications [MERRA]). Model evaluations show that both PS\_BVOC and MEGAN schemes capture reasonable spatial patterns of the global isoprene emissions. The averaged fluxes from simulations using two meteorological forcings show isoprene trends of 0.69 Tg C m<sup>2</sup> a<sup>-1</sup> with PS\_BVOC scheme but −0.22 Tg C m<sup>2</sup> a<sup>-1</sup> with MEGAN scheme. Such opposite trend is mainly because PS\_BVOC considers both CO<sub>2</sub> fertilization and inhibition effects to isoprene while the MEGAN scheme implements CO<sub>2</sub> inhibition effect alone. Meanwhile, the averaged fluxes from simulations using two schemes yield interannual variability of 1.59% with WFDEI and 2.06% with MERRA reanalyses. Such discrepancies are mainly attributed to the larger variability in MERRA data. On the global scale, differences in schemes are the main driver of uncertainties in isoprene trends. In contrast, differences in meteorological forcings dominate the uncertainties in the interannual variability of isoprene emissions. Our sensitivity experiments reveal the key sources of modeling uncertainties, which are vital for the improvement of parameterizations and future projections of isoprene emissions.

## 1. Introduction

Volatile organic compounds (VOC) from natural vegetation comprise about 90% of global terrestrial non-methane VOC emissions annually (Fuentes et al., 2000). Biogenic VOCs (BVOCs) play an important role in the formation of secondary organic aerosols (Claeys, Graham, et al., 2004; Claeys, Wang, et al., 2004) and tropospheric ozone at high light intensities and temperatures in the presence of NO<sub>x</sub> (Fu & Liao, 2012; Wolfe et al., 2011). BVOCs also cause a decrease in atmospheric hydroxyl radical (OH) concentrations and thus result in an increase of the lifetime of methane (CH<sub>4</sub>) in the troposphere (Poisson et al., 2000; Roelofs & Lelieveld, 2000), which can further lead to important feedbacks to both emissions and climate (Kulmala et al., 2004; Penuelas & Llusia, 2003).

Isoprene (2-methyl-1,3-butadiene, C<sub>5</sub>H<sub>8</sub>) is a short-lived (minutes to hours) volatile product emitted from a large number of plants, comprising about half of the global total BVOC (Guenther et al., 2012). Isoprene emissions are highly dependent on vegetation characteristics and weather conditions. Forest emissions are usually much larger than farmland (Hantson et al., 2017; Harper & Unger, 2018; Unger, 2014). Higher temperature and more light promote isoprene emissions (Hantson et al., 2017; Penuelas & Llusia, 2003; Zhang et al., 2008). Carbon dioxide promotes photosynthesis but suppress isoprene emissions (Arneeth et al., 2007; Hantson et al., 2017; Possell & Hewitt, 2011; Unger et al., 2013; Young et al., 2009).

Furthermore, environmental stresses such as drought and surface ozone also affect isoprene emissions (Calafapietra et al., 2013; Llusia et al., 2002; Wolfe et al., 2011).

Several isoprene emission schemes have been developed based on the observed relationships between BVOC emissions and environmental factors. For example, Guenther et al. (2006) proposed the Model of Emissions of Gases and Aerosols from Nature (MEGAN) taking into account the positive effects of warming and light on emissions. Other models are also developed by considering the effects of energy and photosynthetic processes (Arneth et al., 2007; Grote & Niinemets, 2008; Niinemets et al., 1999; Unger et al., 2013). However, predicted emissions vary significantly from study to study, due to the differences in spatiotemporal scales, physical parameterizations, and meteorological driving fields. Such uncertainties may further cause discrepancies in the predicted air pollutants (Guenther et al., 2006, 2012; Jiang et al., 2013; Wu et al., 2008).

There have been several studies exploring the uncertainties in the estimate of isoprene emissions. Lamb et al. (1987) found that emission schemes are the dominant contributor (200%) of uncertainties to their compiled US BVOC emission inventory, much higher than the rates of 30%–55% by measurements, 25% by biomass densities, and 15% by land use distributions. Arneth et al. (2011) compared three models with different inputs and found that the sensitivities to combined vegetation fields and climate inputs are larger than that to individual variables, especially for the simulated seasonality of emission patterns. Guenther et al. (2012) pointed that the uncertainties from the emission factors are the largest contributor to the overall BVOC emission uncertainty, followed by the comparable magnitude of uncertainties from land cover and meteorological driving variables. However, other studies identified meteorological forcings, including soil moisture (Jiang et al., 2018; Monson et al., 2012), air temperature and radiation (Huang et al., 2017) are the major sources of emission uncertainties. These studies are performed using different meteorological forcings and/or emission schemes at varied spatiotemporal scales, making it difficult to compare their conclusions.

In this study, we perform global simulations of isoprene emissions using the Yale Interactive terrestrial Biosphere (YIBs) model (Yue, Unger, & Zheng, 2015), which is implemented with two emission schemes of isoprene and driven by two long-term reanalysis meteorology. We compare the contributions of emission schemes and meteorological forcings to the uncertainties in the simulated trend and variability of isoprene emissions within the same model framework. Both the YIBs model and schemes will be described in the next section. Simulated isoprene emissions are evaluated and analyzed in Section 3. The uncertainties of emissions are further explored in Section 4.

## 2. Method and Data

### 2.1. Observational and Reanalysis Data Sets

#### 2.1.1. Isoprene Emissions

We collected measurements of isoprene emissions from literature (Table S1) through the Web of Science (<https://apps.webofknowledge.com>) using keywords like isoprene/BVOCs and measurement/observation/flux. More than three hundred literatures were found, among which 56 papers provided site locations, observational periods, and emission fluxes. For these selected papers, average emissions in the texts or tables were collected directly, while fluxes in graphs were extracted with GetData software (version 2.22). The units of all emissions were uniformly converted to  $\text{mg C m}^{-2} \text{ day}^{-1}$  so as to facilitate the comparisons with simulations. In total, 113 data samples were collected with some repeated locations conducted by different researchers. We then calculated the average emission fluxes from different observational sources at the same site. Finally, literature-based measurements were compiled at 50 sites, including 17 evergreen broadleaf forest (EBF), six evergreen needleleaf forest (ENF), 21 deciduous broadleaf forest (DBF), one shrubland (shrub), four grassland (grass), and one cropland (crop) (Figure 1a).

#### 2.1.2. Meteorological Input Data Sets

Two meteorological reanalyses are used as input for the vegetation model. The WATCH forcing data (WFD) methodology applied to ERA-Interim data (WFDEI; Weedon et al., 2014) is an update of the WFD, which is developed from the European Center for Medium-range Weather Forecasts (ECMWF) ERA-40 reanalysis (Uppala et al., 2005). Meteorological variables applied include surface air temperature, specific humidity,

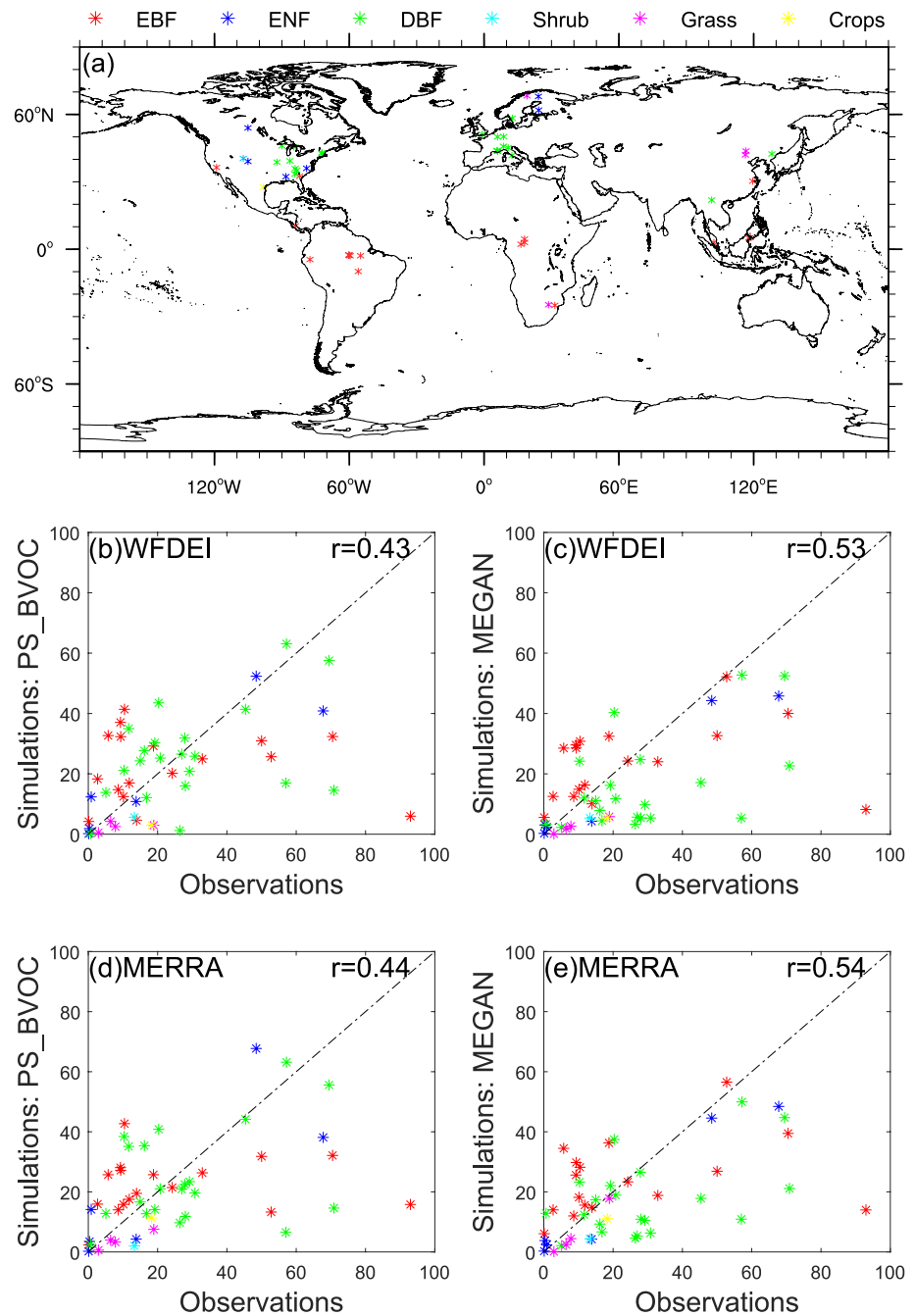


**Figure 1.** Distribution of observational records and their comparisons with YIBs simulations. Literature-based measurements are collected from (a) 50 sites, including 17 evergreen broadleaf forest, six evergreen needleleaf forest, 21 deciduous broadleaf forest, one shrubland (shrub), four grassland (grass), and one cropland (crop). These observations are compared with simulations from (b and d) PS\_BVOC and (c and e) Model of Emissions of Gases and Aerosols from Nature schemes driven with WFDEI (b and c) or Modern-Era Retrospective Analysis for Research and Applications (d and e) reanalysis. Units:  $\text{mg C m}^{-2} \text{ day}^{-1}$ . The correlation coefficients ( $r$ ) are shown in each plot.

wind speed, surface pressure, downward radiation flux, and soil temperature and wetness. For this study, we use WFDEI data from 1980 to 2015 at 3-hour interval, which is linearly interpolated to hourly time step. All the forcing data are interpolated to the  $1^\circ \times 1^\circ$  spatial resolution.

The other data set is from Modern-Era Retrospective Analysis for Research and Applications (MERRA), which is a reanalysis product generated by the National Aeronautics and Space Administration (NASA)

Global Modeling and Assimilation Office (GMAO) using the Goddard Earth Observing System (GEOS) version 5.2.0 (Rienecker et al., 2011; <http://gmao.gsfc.nasa.gov/research/MERRA/>). Similar to WFDEI, MERRA product also provides estimates of land surface fields, including surface meteorological forcing data (such as precipitation, radiation, air temperature, and humidity) and land surface states and fluxes (such as soil moisture, snow, and runoff). For this study, we use MERRA data from 1980 to 2015 at hourly time step and  $1^\circ \times 1.333^\circ$  by latitude and longitude. Trends (variability) of major meteorological fields, including temperature, photosynthetically active radiation (PAR), and soil moisture from both WFDEI and MERRA are shown in Figure S1 (Figure S2).

## 2.2. YIBs Vegetation Model

The YIBs model is a process-based vegetation model that can dynamically simulate plant photosynthesis and isoprene emissions (Yue & Unger, 2015). It considers the biological processes of nine plant functional types (PFTs) including tundra, C<sub>3</sub>/C<sub>4</sub> grass, shrubland, DBF, ENF, EBF and C<sub>3</sub>/C<sub>4</sub> cropland. The vegetation biophysics calculates leaf-level photosynthesis using the well-established Farquhar scheme (Caemmerer & Farquhar, 1981; Farquhar et al., 1980) and the stomatal conductance model of Ball and Berry (Collatz et al., 1991). The vegetation biophysics also consider soil water stress following the approach of Porporato et al. (2001). The two-leaf radiative transfer scheme separates the sunlit and shaded leaves and computes direct and diffuse PAR for both of them. The unique feature of YIBs is the implementation of two schemes (PS\_BVOC or MEGAN) for isoprene emission (Yue, Unger, & Zheng, 2015). The YIBs is driven with global meteorological reanalyses (WFDEI or MERRA) and observed CO<sub>2</sub> concentrations. Simulated carbon fluxes and leaf area index have been extensively evaluated against both site-level observations (Yue & Unger, 2015) and satellite retrievals (Yue, Unger, Keenan, et al., 2015).

## 2.3. Isoprene Emission Schemes

### 2.3.1. Photosynthesis-Dependent Scheme (PS\_BVOC)

The PS\_BVOC scheme calculates isoprene emissions as a function of the electron transport-limited photosynthesis rate, canopy temperature, and intercellular CO<sub>2</sub> concentrations (Arneeth et al., 2007; Niinemets et al., 1999; Unger et al., 2013). The leaf-level isoprene emission rate ( $I_p$ ) is calculated as follows (units:  $\mu\text{mol m}^{-2}$  [leaf] s<sup>-1</sup>):

$$I_p = J_e \cdot \beta \cdot \kappa_p \cdot \tau \cdot \varepsilon \quad (1)$$

where  $J_e$  is the electron transport limited photosynthesis rate (units:  $\mu\text{mol m}^{-2}$  [leaf] s<sup>-1</sup>), depending on the incident PAR and the internal leaf CO<sub>2</sub> concentration ( $C_i$ ):

$$J_e = a_{\text{leaf}} \cdot \text{PAR} \cdot \alpha_{\text{qe}} \cdot \frac{C_i - \Gamma^*}{C_i + 2\Gamma^*} \quad (2)$$

where  $a_{\text{leaf}}$  is the leaf-specific light absorbance and  $\alpha_{\text{qe}}$  is the intrinsic quantum efficiency for photosynthetic CO<sub>2</sub> uptake (Unger et al., 2013).  $\Gamma^*$  is the CO<sub>2</sub> compensation point at which leaf photosynthesis is fully offset by respiration (Collatz et al., 1991).

The  $\beta$  term in Equation 1 is a factor converting electron flux to isoprene equivalents:

$$\beta = \frac{C_i - \Gamma^*}{6(4.67C_i + 9.33\Gamma^*)} \quad (3)$$

Both the changes of  $J_e$  and  $\beta$  are dependent on  $C_i$ , which is regulated by soil moisture. The atmospheric CO<sub>2</sub>-inhibition is included via a parameterization ( $\kappa_p$ ):

$$\kappa_p = \frac{C_{i\_standard}}{C_i} \quad (4)$$

where  $C_{i\_standard}$  ( $=0.7 \times 370$ ) is the leaf  $C_i$  at the standard ambient CO<sub>2</sub> of 370 ppmv for the year 2000 (Wilkinson et al., 2009). Both the short-term and long-term responses of isoprene emissions from intercellular CO<sub>2</sub> (Equations 2 and 3) to changes in atmospheric CO<sub>2</sub> concentration (Equation 4) have been considered respectively (Heald et al., 2009; Wilkinson et al., 2009). For example, the short-term increase of CO<sub>2</sub>



can inhibit stomatal conductance, leading to smaller  $C_i$  and the consequent lower  $I_p$ . On the other hand, the long-term  $\text{CO}_2$  fertilization promotes  $C_p$ , leading to higher  $I_p$  on the long run.

The temperature factor ( $\tau$ ) accounts for the difference in the optimal temperature between photosynthesis and isoprene synthase:

$$\tau = \exp\left[0.1(T - T_{\text{ref}})\right] \quad (5)$$

where  $T$  is leaf temperature and  $T_{\text{ref}}$  is the standard temperature of 30°C.

$\mathcal{E}$  (unitless) is the PFT-specific fraction of electrons available for isoprene synthesis or isoprene emission potential which is calculated by use of available PFT-specific standard leaf isoprene emission rates from observations (Unger et al., 2013).

### 2.3.2. MEGAN Scheme

The MEGAN scheme has been applied widely in the estimates of global isoprene emissions (Guenther et al., 2006, 2012; Situ et al., 2014). It calculates isoprene emissions based on variations driving the major processes including a light response based on electron transport (Guenther et al., 1991), a temperature response due to enzymatic activity (Guenther et al., 1991), and a  $\text{CO}_2$  response caused by changes in metabolism, enzyme and gene expression (Wilkinson et al., 2009). The leaf-level isoprene emission rate ( $I_M$ ) is calculated as follows (units:  $\mu\text{mol Cm}^{-2}\text{s}^{-1}$ ):

$$I_M = I_S \cdot C_{PAR} \cdot C_T \cdot \kappa_m \cdot C_{sm} \quad (6)$$

where  $I_S$  is the PFT-specific isoprene emission potential (units:  $\mu\text{molCm}^{-2}\text{s}^{-1}$ ) similar to  $\mathcal{E}$  in PS\_BVOC.  $C_{PAR}$  is the function of PAR,  $C_T$  is related to leaf temperature,  $\kappa_m$  is determined by atmospheric  $\text{CO}_2$  concentration that accounts for the inhibition effect and  $C_{sm}$  is a multiplier value between 0 and 1 to account for soil moisture availability:

$$C_{PAR} = \frac{\alpha C_{L1} PAR}{\sqrt{1 + \alpha^2 (PAR)^2}} \quad (7)$$

$$C_T = \frac{\exp\left(\frac{C_{T1}(T_K - T_{K_s})}{RT_{K_s} T_K}\right)}{1 + \exp\left(\frac{C_{T2}(T_K - T_M)}{RT_{K_s} T_K}\right)} \quad (8)$$

$$\kappa_m = 1.344 - \frac{1.344 \cdot (0.7C_a)^{1.4614}}{585^{1.4614} + (0.7C_a)^{1.4614}} \quad (9)$$

$$C_{sm} = \begin{cases} 1 & \theta > \theta_1 \\ \frac{\theta - \theta_w}{\theta_1 - \theta_w} & \theta_w < \theta < \theta_1 \\ 0 & \theta < \theta_w \end{cases} \quad (10)$$

$T_K$  is leaf temperature (units: K),  $T_{K_s}$  is the standard leaf temperature of 303 K,  $C_a$  is environmental  $\text{CO}_2$  concentration and  $R$  is the ideal gas constant ( $8.314 \text{ J K}^{-1} \text{ mol}^{-1}$ ).  $\alpha$  (0.0027),  $C_{L1}$  (1.066),  $C_{T1}$  ( $95,000 \text{ J mol}^{-1}$ ),  $C_{T2}$  ( $230,000 \text{ J mol}^{-1}$ ) and  $T_M$  (314 K) are empirical coefficients. Parameter  $C_{sm}$  is calculated based on volumetric soil water content  $\theta$  provided by climate models or reanalyses in six soil layers (Equation 10). The value of  $C_{sm}$  varies from no water stress (=1) to the soil moisture stress onset point ( $\theta_1$ ) through to the wilting point ( $\theta_w$ ), below which  $C_{sm}$  becomes 0 with no isoprene emissions (Porporato et al., 2001). The PS\_BVOC scheme applies the same  $C_{sm}$  parameter to regulate stomatal conductance, and the consequent  $C_i$  (Unger et al., 2013; Zheng et al., 2015).

**Table 1**

*Summary of Simulations Driven With WFDEI and Modern-Era Retrospective Analysis for Research and Applications (MERRA) Reanalyses*

Simulations	MET	CO <sub>2</sub>	T	PAR	SOILM
WFDEI_CTRL	1980–2015	1980–2015	1980–2015	1980–2015	1980–2015
WFDEI_MET	1980	1980–2015	1980	1980	1980
WFDEI_CO2	1980–2015	1980	1980–2015	1980–2015	1980–2015
WFDEI_COT	1980–2015	1980	1980	1980–2015	1980–2015
WFDEI_CO2P	1980–2015	1980	1980–2015	1980	1980–2015
WFDEI_CO2S	1980–2015	1980	1980–2015	1980–2015	1980
MERRA_CTRL	1980–2015	1980–2015	1980–2015	1980–2015	1980–2015
MERRA_MET	1980	1980–2015	1980	1980	1980
MERRA_CO2	1980–2015	1980	1980–2015	1980–2015	1980–2015
MERRA_CO2T	1980–2015	1980	1980	1980–2015	1980–2015
MERRA_CO2P	1980–2015	1980	1980–2015	1980	1980–2015
MERRA_CO2S	1980–2015	1980	1980–2015	1980–2015	1980

The leaf-scale isoprene emissions ( $I$ ) in both schemes are upscaled to the canopy scale isoprene emissions ( $E$ ) by integrating over each canopy layer as follows:

$$E = \int_0^{\text{LAI}} I \, dL \quad (11)$$

Here  $dL$  is the leaf area index (LAI) of individual canopy layers. The total LAI is calculated in YIBs model on a daily basis as follows:

$$\text{LAI} = f \times \text{LAI}_b \quad (12)$$

where  $f$  is the phenological factor, and  $\text{LAI}_b$  is the biomass balanced LAI related to tree height. Dynamic LAI is simulated during 1980–2015, and has been evaluated with available observations in Yue and Unger (2015) and multi-model inter-comparisons in Friedlingstein et al. (2020). At the leaf scale, the PS\_BVOC scheme includes both CO<sub>2</sub> fertilization and inhibition effects (Equations 2–4), while MEGAN scheme applies the inhibition effect alone (Equation 9). At the canopy scale, isoprene emissions are indirectly related to CO<sub>2</sub> fertilization effects via changes of LAI for both schemes, though such indirect effects are much smaller in magnitude compared to the direct CO<sub>2</sub> fertilization effects (Yue, Unger, & Zheng, 2015).

## 2.4. Simulations

We focus on the trend and interannual variability of global isoprene emissions from 1980 to 2015. The trend is calculated as the regression of emission fluxes to the temporal range (1980–2015). The interannual variability is calculated as the ratio (in percentage) between one standard deviation and long-term annual mean fluxes. We perform 12 sensitivity simulations to identify driving factors for the trend and interannual variability (Table 1). These simulations can be separated into two groups, one is driven with WFDEI and the other is driven with MERRA reanalysis. For each group, a control simulation (CTRL) is performed using interannually varied meteorology and CO<sub>2</sub> concentrations ( $[\text{CO}_2]$ ) for 1980–2015. The “MET” run is the same as the control simulation but prescribes all meteorological variables at the year 1980, and the “CO2” run prescribes  $[\text{CO}_2]$  at the year 1980 with other variables interannually varying. To isolate the impact of individual meteorological variables, three additional runs are performed with fixed  $[\text{CO}_2]$  at the year 1980 and one meteorological field recycling for 1980, such as temperature (CO2T), PAR (CO2P), or soil moisture (CO2S), but others vary interannually. For each iteration of each simulation, two isoprene schemes are called, and the derived emissions are output separately.

The differences between CTRL and CO2 (MET) represent the impacts of CO<sub>2</sub> (meteorological) changes to the spatiotemporal variations in isoprene emissions. The differences between CO2 and CO2T isolate

the effects of temperature changes. Similarly, CO2P and CO2S quantify the impacts of radiation and soil moisture, respectively. By comparing the results from two groups, we assess the uncertainties in simulated isoprene emissions caused by meteorological forcings (WFDEI vs. MERRA). By comparing the results from two schemes, we quantify the uncertainties associated with schemes (PS\_BVOC vs. MEGAN). Results from 1982 to 2015 are used for analyses with the first two spin-up years. The resolution of the modeling is  $1^\circ \times 1^\circ$  by latitude and longitude using WFDEI and  $1^\circ \times 1.333^\circ$  using MERRA.

### 3. Results

#### 3.1. Model Evaluation

We first evaluate the simulated isoprene emissions from different schemes driven with different meteorological forcings (Figure S3). Observations are collected from literature with six main PFTs over the world, mainly distributed in North America, Amazon, and Europe (Figure 1a). Simulated isoprene emissions are interpolated to the specific locations where the measurement samples are collected and averaged for the same observing periods. The correlation coefficients are 0.53–0.54 ( $p < 0.05$ ) between observations and simulations using the MEGAN scheme, higher than the values of 0.43–0.44 ( $p < 0.05$ ) derived for simulations using the PS\_BVOC scheme. In general, the differences of meteorological forcings cause limited impacts on the modeled spatial pattern.

The relatively lower correlations for PS\_BVOC than that for MEGAN are caused by the biases in several sites. For example, one EBF site (Alta Floresta, Mato Grosso in the southern Amazon) shows observed emissions of  $52.8 \text{ mg C m}^{-2} \text{ day}^{-1}$ , and the simulation yields a close estimate of  $52.2\text{--}56.5 \text{ mg C m}^{-2} \text{ day}^{-1}$  using the MEGAN scheme. However, the predicted value is much lower at  $13.3\text{--}25.7 \text{ mg C m}^{-2} \text{ day}^{-1}$  using the PS\_BVOC scheme, leading to lower correlations for this PFT. In addition, simulated average emission is lower by 51.02%–75.5% for grass and crop sites using the PS\_BVOC scheme. Although the simulations using MEGAN scheme also underestimate isoprene emissions for these PFTs, such biases are reduced to 33.98%–70.85%. Except for these two PFTs, the relative mean biases are  $-11.53\% \sim -9.47\%$  for EBF,  $-13.78\% \sim -9.24\%$  for DBF, and  $-9.81\% \sim -2.62\%$  for ENF using the PS\_BVOC scheme, comparable to (or even better than) the values of  $-5\% \sim -2.42\%$ ,  $-44.14\% \sim -38.68\%$ , and  $-23.83\% \sim -21.05\%$  using the MEGAN scheme, suggesting that both PS\_BVOC and MEGAN schemes depict reasonable spatial pattern of the global isoprene emissions.

In addition to site measurements, Fu et al. (2019) and Wells et al. (2020) have retrieved isoprene abundance using the satellite-borne Cross-track Infrared Sounder (CrIS). The correlation coefficients are 0.52–0.54 ( $p < 0.05$ ) between CrIS isoprene and simulations using the MEGAN scheme, higher than the values of 0.51–0.54 ( $p < 0.05$ ) derived for simulations using the PS\_BVOC scheme in April 2013 (Figure S4). The comparisons show that YIBs can capture the isoprene hotspots and seasonal variability in some regions. For example, simulated emissions show peaks in April over Central Africa and in July over southeastern United States, consistent with the CrIs retrieval. However, in western Amazon, YIBs predicts the highest isoprene emissions in October, while CrIs shows maximum values in April. The similar problem has been mentioned in Wells et al. (2020) when CrIs results were compared with GEOS-Chem. In addition, retrieved isoprene shows maximum in the northwest of Amazon, while the model prediction shows maximum in the central region. Such discrepancies may be in part attributed to the differences in isoprene profiles as YIBs simulates canopy-level isoprene emissions while CrIs retrieves column density.

#### 3.2. Trends of Isoprene Emissions

Simulated trends of isoprene emissions are sensitive to the choice of modeling schemes. Driven with WFDEI reanalyses, the PS\_BVOC scheme predicts a global increase of  $0.56 \text{ Tg C a}^{-2}$  during 1982–2015, with the enhancements of  $0.17 \text{ Tg C a}^{-2}$  in southern Africa and  $0.08 \text{ Tg C a}^{-2}$  in Amazon (Figure 2a). Soil moisture is the main driver for the enhancement in southern Africa, while  $\text{CO}_2$  dominates the changes in Amazon (Figure 2b). In contrast, using MEGAN scheme, the YIBs model simulates a global reduction of  $0.06 \text{ Tg C a}^{-2}$  for isoprene emissions (Figure 2c). Strong declines are found in central Africa ( $-0.02 \text{ Tg C a}^{-2}$ ), Amazon ( $-0.01 \text{ Tg C a}^{-2}$ ) and Indonesia ( $-0.06 \text{ Tg C a}^{-2}$ ). Increasing  $[\text{CO}_2]$  promotes photosynthesis but meanwhile inhibits BVOC emissions (Unger et al., 2013). These two opposite effects are offsetting each other, leading to moderate changes of isoprene in tropical rainforest with the PS\_BVOC scheme (Figure 2a). However, the MEGAN scheme does not include the  $\text{CO}_2$  fertilization effects, as a result the  $\text{CO}_2$  enhancement in-

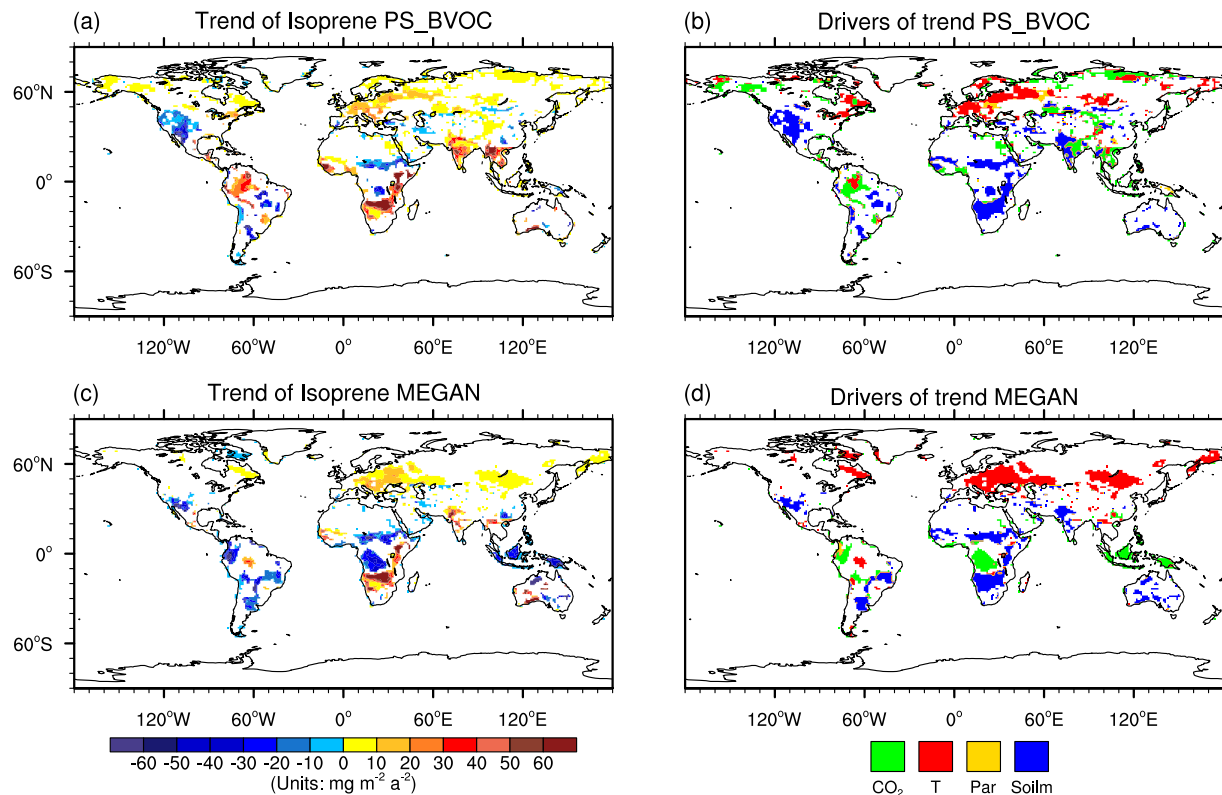


**Figure 2.** Trends of (a and c) isoprene emissions and (b and d) their dominant drivers as simulated with (a and b) PS\_BVOC and (c and d) Model of Emissions of Gases and Aerosols from Nature schemes. The simulations are performed with WFDEI reanalyses during 1982–2015. Four factors, including CO<sub>2</sub>, temperature, photosynthetically active radiation (PAR), and soil moisture, are considered as the potential drivers of flux trends. The factor contributing the largest magnitude to the total trend is denoted for a specific grid. Only significant trends ( $p < 0.05$ ) are presented.

stead reduces isoprene emissions (Equation 9) in central Africa, Amazon and Indonesia (Figure 2d). Except for these discrepancies, the two schemes predict similar isoprene trends elsewhere, including the negative changes in western U.S. and eastern China but positive changes in Europe, India, and South Africa.

Driven with MERRA reanalysis, the PS\_BVOC scheme predicts a global trend of 0.82 Tg C a<sup>-2</sup> for isoprene emissions (Figure 3a). Large enhancements are found in South America (0.54 Tg C a<sup>-2</sup>), while strong reductions are predicted in central Africa (−0.32 Tg C a<sup>-2</sup>). Soil moisture makes the dominant contributions to the emission decline in central Africa (Figure 3b). In contrast, using MEGAN scheme, the YIBs model simulates a global reduction of 0.38 Tg C a<sup>-2</sup> for isoprene emissions (Figure 3c). Strong decline was found in South America (−0.83 Tg C a<sup>-2</sup>), while large enhancement was predicted in central Africa (0.11 Tg C a<sup>-2</sup>), opposite to the predictions with the PS\_BVOC scheme. Temperature rising contributes most to the emission enhancement in Europe and Inner Mongolia (Figure 3d).

### 3.3. Interannual Variability of Isoprene Emissions

Driven with WFDEI reanalyses, PS\_BVOC scheme predicts a global interannual variability of 1.4% during 1982–2015 (Figure 4a). High values are found in Australia (18.9%) and South Africa (25.8%), where soil moisture is the main driver (Figure 4b). As a comparison, using the MEGAN scheme, the YIBs model simulates a larger global interannual variability of 1.8% for isoprene emissions (Figure 4c). However, the variabilities of 9.8% in Australia and 12.4% in southern Africa are lower compared to that predicted by PS\_BVOC. Meanwhile, larger variability is predicted over vast domains such as Russia (5.8% vs. 2.4%) and Europe (4.8% vs. 2.8%) in MEGAN than PS\_BVOC. For the PS\_BVOC scheme, temperature is the main driver at high latitudes (>60°N) while soil moisture makes the dominant contributions at low to middle latitudes (<60°N). For the MEGAN scheme, temperature is the dominant driver almost globally except for arid and semi-arid regions in tropics (Figure 4d).

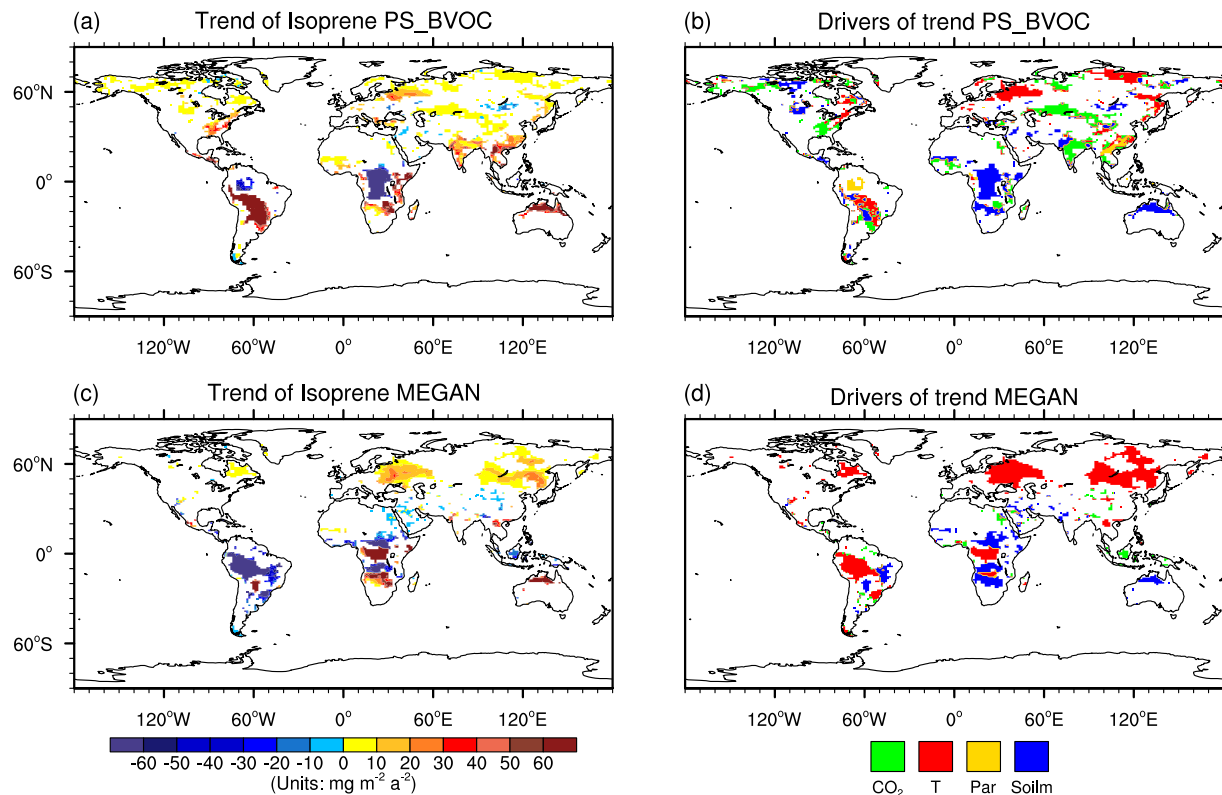


**Figure 3.** The same as Figure 2 but for simulations driven with Modern-Era Retrospective Analysis for Research and Applications reanalysis.

Driven with MERRA reanalyses, PS\_BVOC scheme predicts a global interannual variability of 2.0% during 1982–2015 (Figure 5a). High values are found in Australia (22.8%) and South Africa (17.4%), where soil moisture is again the main driver (Figure 5b). Using MEGAN scheme, the YIBs model simulates a global interannual variability of 2.1% for isoprene emissions (Figure 5c). The variability is lower in Australia (16.6%) and South Africa (5.5%) than that in PS\_BVOC. However, variabilities in Russia and Europe are higher with MEGAN (6.0% and 4.1%) than that with PS\_BVOC (3.0% and 3.6%). Similar to the results using WFDEI reanalyses, the interannual variability of isoprene emissions is more dominated by soil moisture in PS\_BVOC but by temperature in MEGAN schemes.

## 4. Uncertainty Analyses

### 4.1. Uncertainties From Emission Schemes

Although both PS\_BVOC and MEGAN schemes consider the effects of temperature and radiation, they apply different formats of physical processes. Regression analyses show that warming in general increases isoprene emissions with MEGAN scheme (Figure 6d), following the positive dependence of emissions to temperature as depicted by Equation 8. However, the PS\_BVOC scheme shows positive responses at high latitudes but negative ones at low latitudes (Figure 6a). Such responses are related to the photosynthesis rate, which has an optimal temperature of 25°C for most of plant species in the model (Collatz et al., 1991). The warming at tropical regions usually decreases photosynthesis because the ambient temperature is higher than 25°C, while the warming at boreal regions promotes photosynthesis due to the low ambient temperature (Piao et al., 2013). The enhanced (reduced) photosynthesis at high (low) latitudes increases (decreases)  $C_p$ , leading to positive (negative) changes in isoprene emissions in response to warming following Equation 3. On the global scale, isoprene increases by 0.98% for PS\_BVOC and 8.95% for MEGAN schemes in response to 1°C enhancement of surface air temperature.



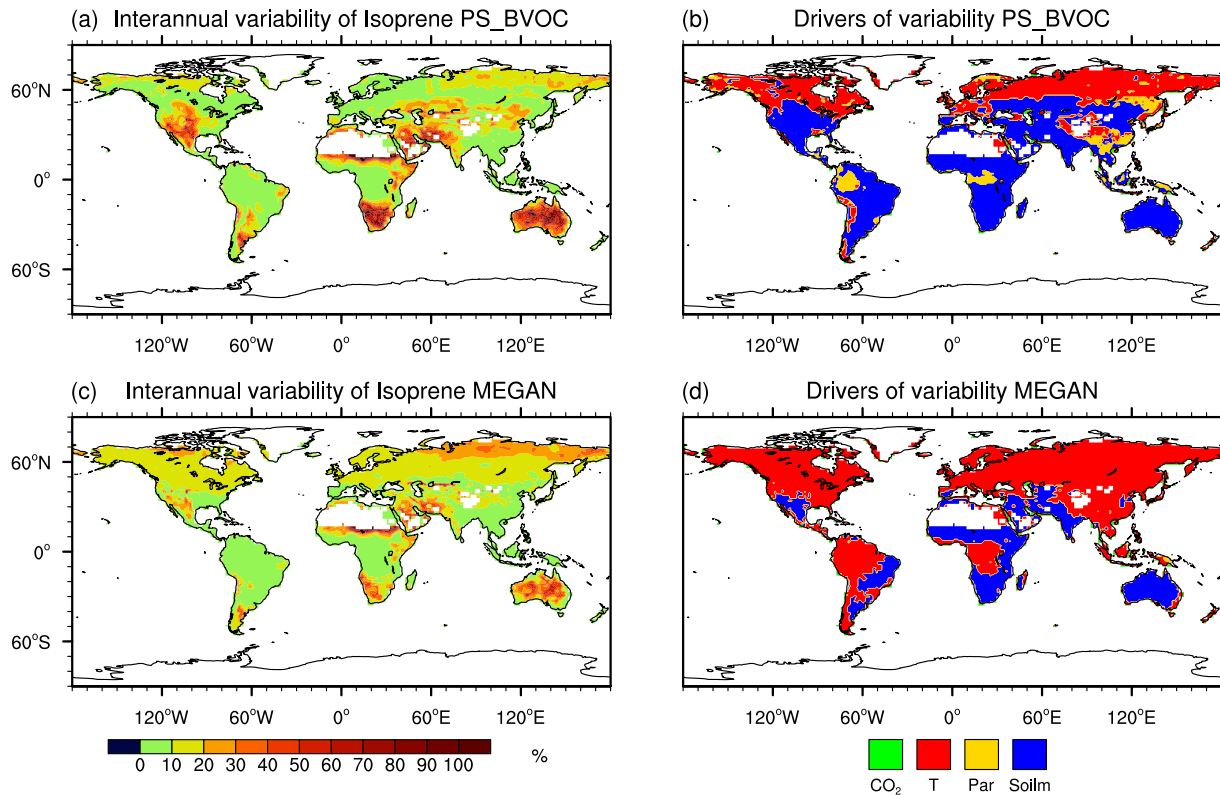


**Figure 4.** Interannual variabilities of (a and c) isoprene emissions and their (b and d) dominant drivers as simulated with (a and b) PS\_BVOC and (c and d) Model of Emissions of Gases and Aerosols from Nature schemes. The simulations are performed with WFDEI reanalysis during 1982–2015. Four factors, including CO<sub>2</sub>, temperature, photosynthetically active radiation, and soil moisture, are considered as the potential drivers of interannual variability. The factor contributing the largest magnitude to the total variability is denoted for each grid. Grids with no color represent no isoprene emissions due to non-veg or non-land types.

Isoprene emissions show widespread enhancement in response to increased PAR for both PS\_BVOC (Figure 6b) and MEGAN (Figure 6e) schemes. Large increases of 1%–3% are predicted at high latitudes in Northern Hemisphere (>40°N) for both schemes. The MEGAN scheme predicts low isoprene enhancement of <1% at low to middle latitudes, where the PS\_BVOC yields widespread changes of >1% except for northern Africa and South America. On the global scale, isoprene increases by 0.80% for PS\_BVOC and 0.42% for MEGAN in response to 1 W m<sup>-2</sup> enhancement of PAR.

Both schemes consider soil water stress following the approach of Porporato et al. (2001) in the vegetation biophysics (Equation 10). As a result, the two schemes show similar patterns of isoprene responses ( $R = 0.9$ ) to soil moisture (Figures 6c and 6f). When soil water is adequate, no water stress is applied for isoprene emissions. However, if soil water is low, stomatal conductance is reduced and thus inhibits isoprene emissions by limiting  $C_1$  values for PS\_BVOC and  $C_{sm}$  term for MEGAN schemes. The largest positive changes over tropical regions (especially in southern Africa, northern India, and Australia) are found, where photosynthesis is limited by water stress. Soil moisture is increasing in these three areas (Figures S1c and S1f), leading to increased isoprene emissions over there in the past 3 decades (Figures 2 and 3). Compared to MEGAN (Figure 6f), predicted soil-moisture-induced isoprene enhancement area is slightly larger for PS\_BVOC scheme (Figure 6c), likely because soil moisture also promotes local photosynthesis that is, benefit for isoprene emissions in the latter scheme. On the global scale, isoprene increases by 2.82% for PS\_BVOC and 1.57% for MEGAN in response to 1% increase of soil moisture.

Both schemes consider CO<sub>2</sub> effects, which dominate the long-term trends of isoprene emissions (Figure 7 and Table S2). The PS\_BVOC scheme includes CO<sub>2</sub> fertilization and inhibition (Equations 2–4), while MEGAN scheme applies the inhibition effect alone (Equation 9). As a result, increased CO<sub>2</sub> promotes isoprene

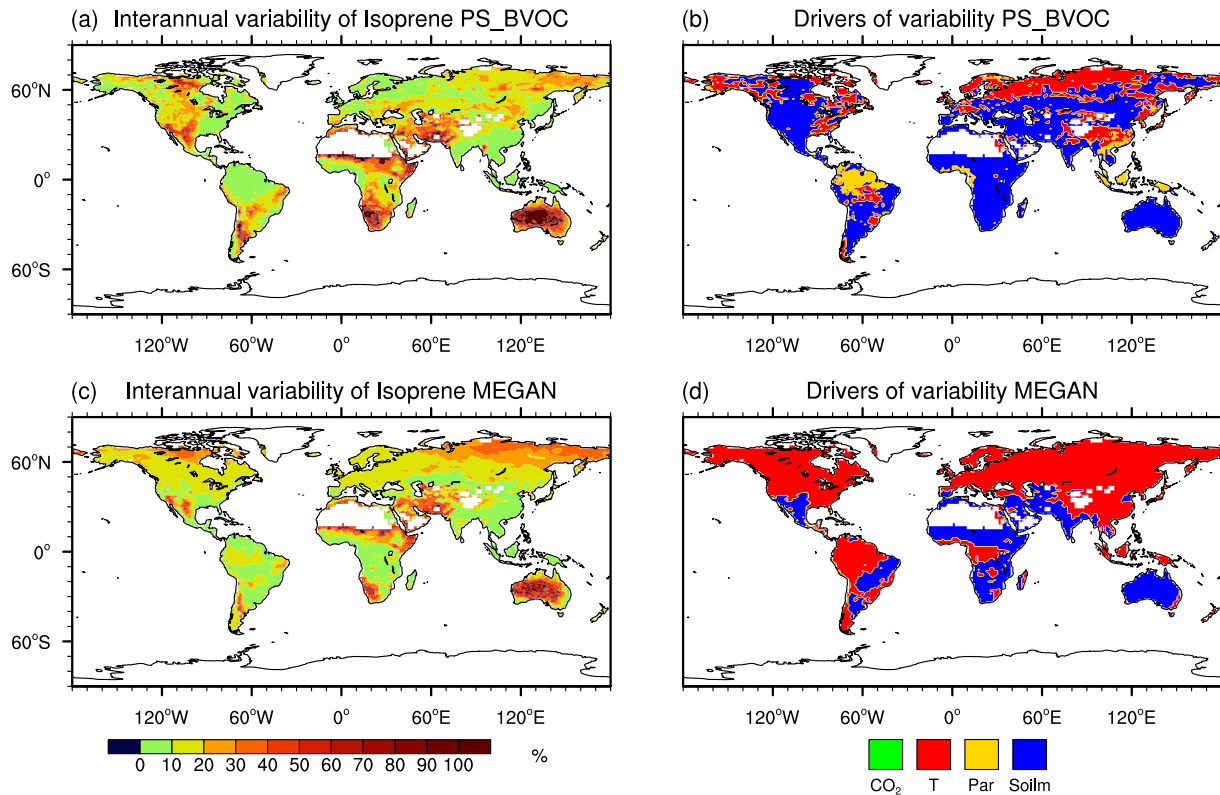


Figure 5. The same as Figure 4 but for simulations driven with Modern-Era Retrospective Analysis for Research and Applications reanalysis.

emissions with the PS\_BVOC scheme but decreases isoprene with the MEGAN scheme during 1982–2015. Such differences in CO<sub>2</sub> effects dominate the scheme uncertainties in the simulated trends of isoprene emissions (Figures 7a and 7b). In contrast, meteorology plays much more important roles than CO<sub>2</sub> effects

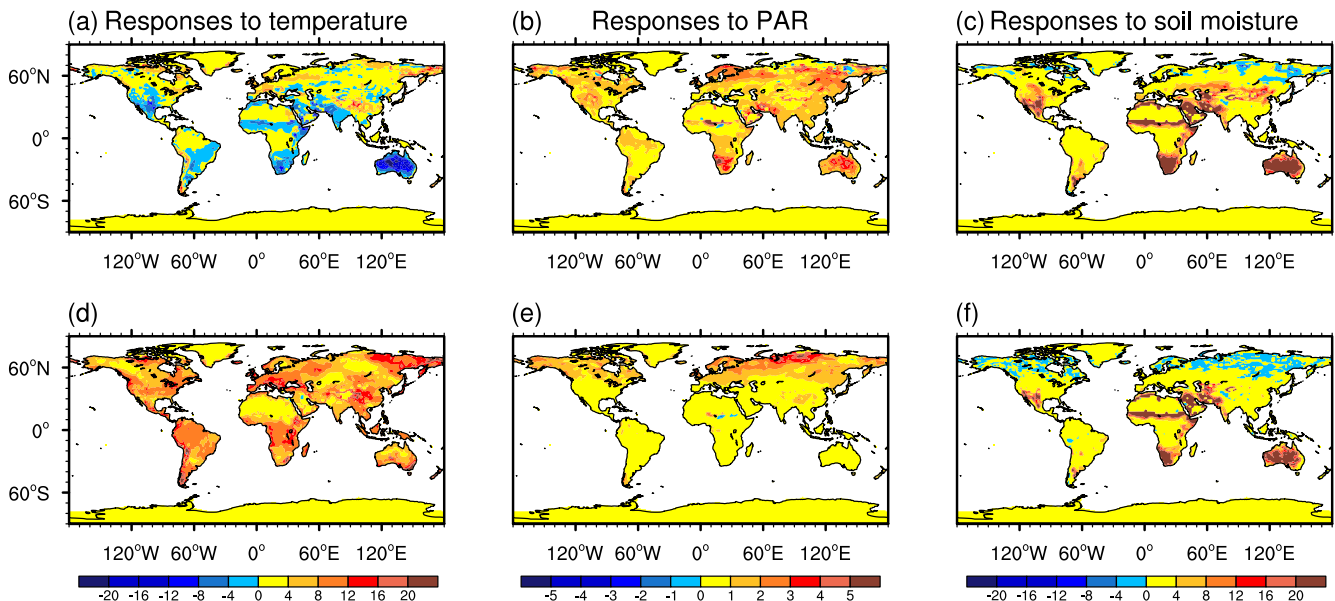
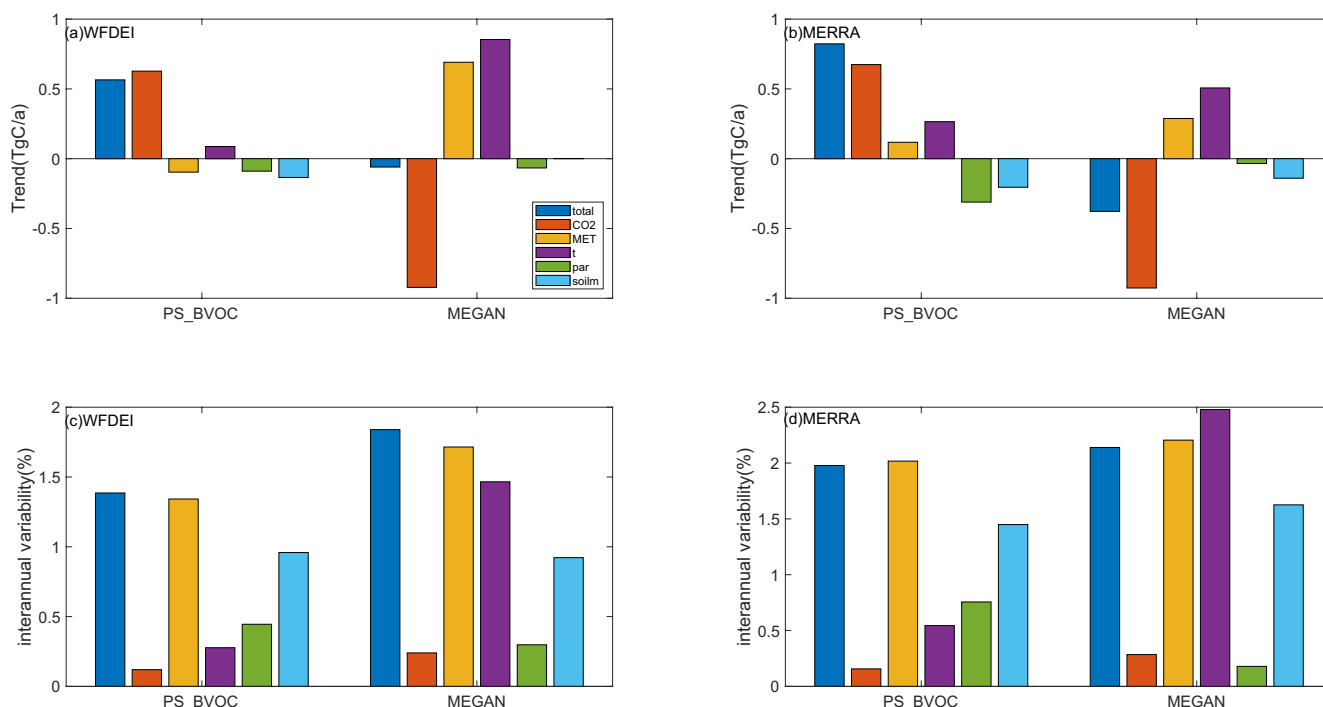


Figure 6. Relationship maps of isoprene to (a and d) temperature ( $\% K^{-1}$ ) (b and e) PAR ( $\% W^{-1}$ ) and (c and f) soil moisture ( $\% 0.01^{-1}$ ), simulated with (a–c) PS\_BVOC and (d–f) Model of Emissions of Gases and Aerosols from Nature schemes. The simulations are driven with WFDEI reanalysis during 1982–2015. Relationship maps derived using Modern-Era Retrospective Analysis for Research and Applications reanalysis are shown in Figure S5.



**Figure 7.** Attribution of the driving factors for (a and b) trends and (c and d) interannual variability as simulated with (a and c) WFDEI or (b and d) Modern-Era Retrospective Analysis for Research and Applications reanalysis. Different colors represent varied drivers, including CO<sub>2</sub>, meteorology, individual meteorological factors such as temperature, photosynthetically active radiation, soil moisture. The joint effect shown in dark blue bar is derived from the control run and is not the additive of individual effects. For each panel, isoprene emissions simulated with PS\_BVOC and Model of Emissions of Gases and Aerosols from Nature schemes are compared. The number of each bar is summarized in Table S2.

in the simulated variability of isoprene emissions (Figures 7c and 7d), though individual variables (such as temperature) may have different magnitude of contributions for the two schemes.

#### 4.2. Uncertainties From Meteorological Forcings

Meteorological fields from WFDEI and MERRA reanalyses show similar trends at middle to high latitudes but inconsistent changes at low latitudes (e.g., central Africa and Amazon) during 1982–2015 (Figure S1). Meanwhile, MERRA reanalyses exhibit larger interannual variability, especially over the tropical regions, than WFDEI data (Figure S2). Such differences in climate forcings lead to discrepancies in both the trends and variability of simulated isoprene emissions (Figure 7).

With fixed CO<sub>2</sub> (MET run), simulated isoprene emissions with PS\_BVOC scheme yields a negative trend of  $-0.1$  Tg C/a using WFDEI reanalyses (Figure 7a). Such trend is jointly contributed by a positive change of  $0.09$  Tg C/a by temperature and negative changes of  $-0.09$  Tg C/a by PAR and  $-0.13$  Tg C/a by soil moisture, following positive trends in temperature (Figure S1a) but negative trends in PAR (Figure S1b) and soil moisture (Figure S1c). In contrast, the same PS\_BVOC scheme yields a positive trend of  $0.12$  Tg C/a in isoprene emissions with MERRA reanalyses when CO<sub>2</sub> is fixed (Figure 7b), mainly because temperature in MERRA has a large increase in central Africa (Figure S1d) and results in a larger positive global isoprene emission trend of  $0.27$  Tg C/a than that in WFDEI. With MEGAN scheme and fixed CO<sub>2</sub>, simulated isoprene shows positive trends of  $0.69$  Tg C/a with WFDEI and  $0.29$  Tg C/a with MERRA reanalyses (Figures 7a and 7b). The larger trend with WFDEI is likely because regional cooling over South America in MERRA reanalyses limits the global increasing trend of isoprene emissions.

Variability of isoprene emissions shows similar features between simulations with the two meteorological forcings, though the magnitude is larger with MERRA (Figure 7d) than that with WFDEI reanalyses (Figure 7c). Such discrepancy is because meteorological fields have larger interannual variability in MERRA (Figures S2d–S2f) than that in WFDEI (Figures S2a–S2c) reanalyses. For PS\_BVOC scheme, soil moisture

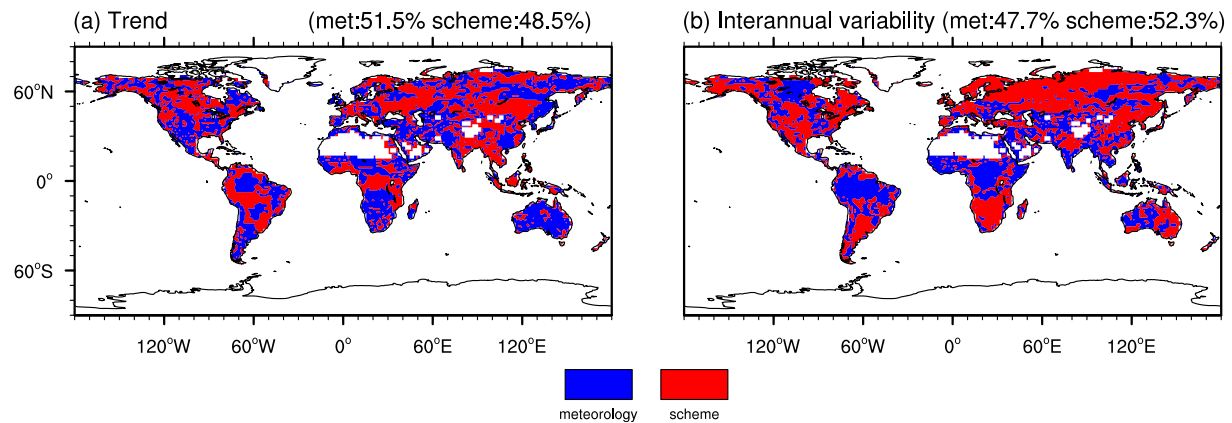


**Figure 8.** Dominant driver (meteorology or scheme) of the uncertainties in (a) trends and (b) interannual variabilities at individual grids. Grid percentage of the main driver is shown in the upper right corner. Grids with no color represent no isoprene emissions due to non-veg or non-land types.

is the main driver with contributions of 1.0% for WFDEI and 1.4% for MERRA reanalyses, followed by PAR (0.5%–0.7%) and temperature (0.3%–0.5%). These contributions result from the largest variability of soil moisture (Figures S2c and S2f), followed by PAR (Figures S2b and S2e) and temperature (Figures S2a and S2d). For MEGAN scheme, temperature makes the dominant contributions to isoprene variability of 1.5% for WFDEI and 2.5% for MERRA, followed by soil moisture (0.9%–1.5%) and PAR (0.2%–0.3%), mainly because MEGAN scheme is more sensitive to temperature (Figure 6d).

#### 4.3. Comparisons of Uncertainties From Schemes and Meteorology

We compare the contributions of emission schemes and meteorological forcings to the uncertainties of trends and variability in simulated isoprene emissions. Globally, the average trend of isoprene emissions between PS\_BVOC and MEGAN simulations is  $0.25 \text{ Tg C m}^2 \text{ a}^{-1}$  with WFDEI and  $0.22 \text{ Tg C m}^2 \text{ a}^{-1}$  with MERRA reanalyses, leading to a meteorology-induced difference of  $0.03 \text{ Tg C m}^2 \text{ a}^{-1}$ . Meanwhile, the average of WFDEI and MERRA simulations yield isoprene trends of  $0.69 \text{ Tg C m}^2 \text{ a}^{-1}$  for PS\_BVOC scheme and  $-0.22 \text{ Tg C m}^2 \text{ a}^{-1}$  for MEGAN scheme, resulting in a scheme-induced difference of  $0.91 \text{ Tg C m}^2 \text{ a}^{-1}$ . As a result, the difference in schemes dominates the uncertainties ( $0.91 \text{ Tg C m}^2 \text{ a}^{-1} > 0.03 \text{ Tg C m}^2 \text{ a}^{-1}$ ) in the simulations of long-term trend of isoprene emissions. On the other hand, simulations yield interannual variabilities of 1.59% with WFDEI and 2.06% with MERRA reanalyses in isoprene emissions, leading to a meteorology-induced difference of 0.43% for variability. As a comparison, simulations using PS\_BVOC scheme and MEGAN scheme show isoprene variability of 1.69% and 1.92%, resulting in a scheme-induced difference of 0.23%. As a result, the difference in meteorology dominates the uncertainties ( $0.43\% > 0.23\%$ ) in the interannual variability of simulated isoprene emissions.

Regionally, the discrepancies in meteorological forcings dominate the uncertainties in isoprene trend over 51.5% land grids, slightly higher than the ratio of 48.5% caused by schemes (Figure 8a). For interannual variability, the discrepancies in schemes dominate uncertainties in isoprene emissions over 52.3% land grids, higher than the ratio of 47.7% caused by meteorology (Figure 8b). Such conclusion is different from the global statistics, which shows that scheme dominates uncertainties in isoprene trend while meteorology dominates uncertainties in isoprene variability (Figure 7). The main cause for such discrepancy is attributed to the uneven spatial distribution of isoprene emissions. As shown in Figure S3, tropical emissions ( $20^{\circ}\text{S}$ – $20^{\circ}\text{N}$ ) account for 66.3%–70.0% of the global amount. Although meteorology has a wider spatial range of influence than schemes on uncertainty in isoprene trend (Figure 8a), the schemes dominate uncertainties of isoprene trends in tropical regions and as a result become the main driver for global total fluxes. Similarly, meteorological forcings dominate the uncertainties of isoprene variability in tropical hotspots (Figure 8b), consequently dominate the uncertainties of global isoprene variability.

## 5. Conclusions and Discussion

We explored the uncertainties in the trends and interannual variabilities of simulated isoprene emissions originating from two different schemes (PS\_BVOC and MEGAN) versus two different climate forcings (WFDEI and MERRA). Evaluations show that both PS\_BVOC and MEGAN schemes capture reasonable spatial pattern of the global isoprene emissions. For the long-term trends during 1982–2015, simulations using PS\_BVOC scheme show positive trends while those with MEGAN scheme yield negative trends in isoprene emissions, mainly because PS\_BVOC considers both CO<sub>2</sub> fertilization and inhibition effects while the MEGAN scheme implements CO<sub>2</sub> inhibition effect alone. For the interannual variability, differences in climate reanalyses are the main driver of uncertainties in isoprene emissions, likely because variability of meteorological forcing is much larger than that of CO<sub>2</sub> concentrations.

There are some limitations in our research. First, observations are very limited for validations. Isoprene is a short-lived (minutes to hours) compound that vary a lot in both space and time (Guenther et al., 2006). As a result, observations of isoprene from regional to global scales are difficult, limiting the evaluation of emission parameterizations. In this study, we validated the spatial pattern of simulated isoprene emissions (Figure 1) but fail to evaluate their temporal variations, which are important for the explorations of long-term trends and interannual variabilities. Second, the current study compared uncertainties from only two schemes and two climate reanalyses. There have been several schemes for isoprene emissions applying different physical dependences to temperature and light (Arneth et al., 2007; Guenther et al., 2012; Unger et al., 2013). Meanwhile, there are multiple reanalyses data showing varied trends and variabilities (Dee et al., 2011; Uppala et al., 2005; Weedon et al., 2014). Comparisons among more schemes and meteorological forcings can better resolve the uncertainty sources of isoprene emissions. Third, this study does not exclude the impacts of LAI on isoprene emissions. The canopy-level emissions depend on LAI (Equation 11), which is also affected by climate change. As a result, the uncertainties induced by meteorological forcings are jointly contributed by uncertainties in leaf-level isoprene emissions and LAI, the latter of which should be isolated in the future analyses.

Despite these limitations, we identified the main drivers of modeling uncertainties for isoprene emissions. The effects of CO<sub>2</sub> dominate the uncertainties in the long-term trend of isoprene. Many experiments have revealed the strong inhibition effects of CO<sub>2</sub> on isoprene emissions (Feng et al., 2019; Lantz et al., 2019; Rosenstiel et al., 2003). However, these studies are usually performed for instant responses at the leaf level with small spatiotemporal scales. For the long-term and ecosystem-level responses, joint effects of plant growth and photosynthesis enhancement may promote isoprene emissions (Sun et al., 2013). More observations lasting seasons to years over different ecosystems are required to reduce modeling uncertainties in CO<sub>2</sub> effects on isoprene emissions, which are vital for the future projection of isoprene concentrations and the consequent air pollution level.

## Data Availability Statement

The simulated isoprene emissions from two schemes (MEGAN and PS\_BVOC) with two meteorological forcings (WFDEI and MERRA) can be accessed at <https://doi.org/10.5281/zenodo.4781814>.

## References

- Arneth, A., Niinemets, U., Pressley, S., Back, J., Hari, P., Karl, T., et al. (2007). Process-based estimates of terrestrial ecosystem isoprene emissions: Incorporating the effects of a direct CO<sub>2</sub>-isoprene interaction. *Atmospheric Chemistry and Physics*, 7, 31–53. <https://doi.org/10.5194/acp-7-31-2007>
- Arneth, A., Schurgers, G., Lathiere, J., Duhl, T., Beerling, D. J., Hewitt, C. N., et al. (2011). Global terrestrial isoprene emission models: Sensitivity to variability in climate and vegetation. *Atmospheric Chemistry and Physics*, 11(15), 8037–8052. <https://doi.org/10.5194/acp-11-8037-2011>
- Caemmerer, S. V., & Farquhar, G. D. (1981). Some relationships between the biochemistry of photosynthesis and the gas exchange of leaves. *Planta*, 153(4), 376–387. <https://doi.org/10.1007/BF00384257>
- Calfapietra, C., Fares, S., Manes, F., Morani, A., Sgrigna, G., & Loreto, F. (2013). Role of biogenic volatile organic compounds (BVOC) emitted by urban trees on ozone concentration in cities: A review. *Environmental Pollution*, 183, 71–80. <https://doi.org/10.1016/j.envpol.2013.03.012>
- Claeys, M., Graham, B., Vas, G., Wang, W., Vermeylen, R., Pashynska, V., et al. (2004). Formation of secondary organic aerosols through photooxidation of isoprene. *Science*, 303(5661), 1173–1176. <https://doi.org/10.1126/science.1092805>

## Acknowledgments

This work was jointly supported by the National Natural Science Foundation of China (grant no. 41975155), the National Key Research and Development Program of China (grant no. 2019YFA0606802), and the Startup Foundation for Introducing Talent of NUIST.



- Claeys, M., Wang, W., Ion, A. C., Kourtchev, I., Gelencser, A., & Maenhaut, W. (2004). Formation of secondary organic aerosols from isoprene and its gas-phase oxidation products through reaction with hydrogen peroxide. *Atmospheric Environment*, *38*(25), 4093–4098. <https://doi.org/10.1016/j.atmosenv.2004.06.001>
- Collatz, G. J., Ball, J. T., Griivet, C., & Berry, J. A. (1991). Physiological and environmental-regulation of stomatal conductance, photosynthesis and transpiration - A model that includes a laminar boundary-layer. *Agricultural and Forest Meteorology*, *54*(2–4), 107–136. [https://doi.org/10.1016/0168-1923\(91\)90002-8](https://doi.org/10.1016/0168-1923(91)90002-8)
- Dee, D. P., Uppala, S. M., Simmons, A. J., Berrisford, P., Poli, P., Kobayashi, S., et al. (2011). The ERA-Interim reanalysis: Configuration and performance of the data assimilation system. *Quarterly Journal of the Royal Meteorological Society*, *137*, 553–597. <https://doi.org/10.1002/qj.828>
- Farquhar, G. D., Caemmerer, S. V., & Berry, J. A. (1980). A biochemical-model of photosynthetic CO<sub>2</sub> assimilation in leaves of C<sub>3</sub> species. *Planta*, *149*(1), 78–90. <https://doi.org/10.1007/bf00386231>
- Feng, Z. Z., Yuan, X. Y., Fares, S., Loreto, F., Li, P., Hoshika, Y., & Paoletti, E. (2019). Isoprene is more affected by climate drivers than monoterpenes: A meta-analytic review on plant isoprenoid emissions. *Plant, Cell and Environment*, *42*(6), 1939–1949. <https://doi.org/10.1111/pce.13535>
- Friedlingstein, P., O'Sullivan, M., Jones, M. W., Andrew, R. M., Hauck, J., Olsen, A., et al. (2020). Global carbon budget 2020. *Earth System Science Data*, *12*(4), 3269–3340. <https://doi.org/10.5194/essd-12-3269-2020>
- Fu, D., Millet, D. B., Wells, K., Payne, V., Yu, S., Guenther, A., & Eldering, A. (2019). Direct retrieval of isoprene from satellite-based infrared measurements. *Nature Communications*, *10*, 3811. <https://doi.org/10.1038/s41467-019-11835-0>
- Fu, Y., & Liao, H. (2012). Simulation of the interannual variations of biogenic emissions of volatile organic compounds in China: Impacts on tropospheric ozone and secondary organic aerosol. *Atmospheric Environment*, *59*, 170–185. <https://doi.org/10.1016/j.atmosenv.2012.05.053>
- Fuentes, J. D., Lerdau, M., Atkinson, R., Baldocchi, D., Bottenheim, J. W., Ciccioli, P., et al. (2000). Biogenic hydrocarbons in the atmospheric boundary layer: A review. *Bulletin of the American Meteorological Society*, *81*(7), 1537–1576. [https://doi.org/10.1175/1520-0477\(2000\)081<1537:BHITAB>2.3.CO;2](https://doi.org/10.1175/1520-0477(2000)081<1537:BHITAB>2.3.CO;2)
- Grote, R., & Niinemets, U. (2008). Modeling volatile isoprenoid emissions - A story with split ends. *Plant Biology*, *10*(1), 8–28. <https://doi.org/10.1055/s-2007-964975>
- Guenther, A., Jiang, X. Y., Heald, C. L., Sakulyanontvittaya, T., Duhl, T., Emmons, L. K., & Wang, X. (2012). The Model of Emissions of Gases and Aerosols from Nature version 2.1 (MEGAN2.1): An extended and updated framework for modeling biogenic emissions. *Geoscientific Model Development*, *5*(6), 1471–1492. <https://doi.org/10.5194/gmd-5-1471-2012>
- Guenther, A., Karl, T., Harley, P., Wiedinmyer, C., Palmer, P. I., & Geron, C. (2006). Estimates of global terrestrial isoprene emissions using MEGAN (Model of Emissions of Gases and Aerosols from Nature). *Atmospheric Chemistry and Physics*, *6*, 3181–3210. <https://doi.org/10.5194/acp-6-3181-2006>
- Guenther, A., Monson, R., & Fall, R. (1991). Isoprene and monoterpene emission rate variability - Observations with eucalyptus and emission rate algorithm development. *Journal of Geophysical Research*, *96*(D6), 10799–10808. <https://doi.org/10.1029/91jd00960>
- Hantson, S., Knorr, W., Schurgers, G., Pugh, T. A. M., & Arneth, A. (2017). Global isoprene and monoterpene emissions under changing climate, vegetation, CO<sub>2</sub> and land use. *Atmospheric Environment*, *155*, 35–45. <https://doi.org/10.1016/j.atmosenv.2017.02.010>
- Harper, K. L., & Unger, N. (2018). Global climate forcing driven by altered BVOC fluxes from 1990 to 2010 land cover change in maritime Southeast Asia. *Atmospheric Chemistry and Physics*, *18*(23), 16931–16952. <https://doi.org/10.5194/acp-18-16931-2018>
- Heald, C. L., Wilkinson, M. J., Monson, R. K., Alo, C. A., Wang, G. L., & Guenther, A. B. (2009). Response of isoprene emission to ambient CO<sub>2</sub> changes and implications for global budgets. *Global Change Biology*, *15*(5), 1127–1140. <https://doi.org/10.1111/j.1365-2486.2008.01802.x>
- Huang, M., Carmichael, G. R., Crawford, J. H., Wisthaler, A., Zhan, X. W., Hain, C. R., et al. (2017). Biogenic isoprene emissions driven by regional weather predictions using different initialization methods: Case studies during the SEAC(4)RS and DISCOVER-AQ airborne campaigns. *Geoscientific Model Development*, *10*(8), 3085–3104. <https://doi.org/10.5194/gmd-10-3085-2017>
- Jiang, H., Liao, H., Pye, H. O. T., Wu, S., Mickley, L. J., Seinfeld, J. H., & Zhang, X. Y. (2013). Projected effect of 2000–2050 changes in climate and emissions on aerosol levels in China and associated transboundary transport. *Atmospheric Chemistry and Physics*, *13*(16), 7937–7960. <https://doi.org/10.5194/acp-13-7937-2013>
- Jiang, X. Y., Guenther, A. B., Potosnak, M., Geron, C., Seco, R., Karl, T., et al. (2018). Isoprene emission response to drought and the impact on global atmospheric chemistry. *Atmospheric Environment*, *183*, 69–83. <https://doi.org/10.1016/j.atmosenv.2018.01.026>
- Kulmala, M., Suni, T., Lehtinen, K. E. J., Dal Maso, M., Boy, M., Reissell, A., et al. (2004). A new feedback mechanism linking forests, aerosols, and climate. *Atmospheric Chemistry and Physics*, *4*(2), 557–562. <https://doi.org/10.5194/acp-4-557-2004>
- Lamb, B., Guenther, A. B., Gay, D., & Westberg, H. (1987). A national inventory of biogenic hydrocarbon emissions. *Atmospheric Environment*, *21*(8), 1695–1705. [https://doi.org/10.1016/0004-6981\(87\)90108-9](https://doi.org/10.1016/0004-6981(87)90108-9)
- Lantz, A. T., Allman, J., Weraduwaage, S. M., & Sharkey, T. D. (2019). Isoprene: New insights into the control of emission and mediation of stress tolerance by gene expression. *Plant, Cell and Environment*, *42*(10), 2808–2826. <https://doi.org/10.1111/pce.13629>
- Llusia, J., Penuelas, J., & Gimeno, B. S. (2002). Seasonal and species-specific response of VOC emissions by Mediterranean woody plant to elevated ozone concentrations. *Atmospheric Environment*, *36*(24), 3931–3938. [https://doi.org/10.1016/s1352-2310\(02\)00321-7](https://doi.org/10.1016/s1352-2310(02)00321-7)
- Monson, R. K., Grote, R., Niinemets, U., & Schnitzler, J. P. (2012). Modeling the isoprene emission rate from leaves. *New Phytologist*, *195*(3), 541–559. <https://doi.org/10.1111/j.1469-8137.2012.04204.x>
- Niinemetts, U., Tenhunen, J. D., Harley, P. C., & Steinbrecher, R. (1999). A model of isoprene emission based on energetic requirements for isoprene synthesis and leaf photosynthetic properties for Liquidambar and Quercus. *Plant, Cell and Environment*, *22*(11), 1319–1335. <https://doi.org/10.1046/j.1365-3040.1999.00505.x>
- Penuelas, J., & Llusia, J. (2003). BVOCs: Plant defense against climate warming? *Trends in Plant Science*, *8*(3), 105–109. [https://doi.org/10.1016/s1360-1385\(03\)00008-6](https://doi.org/10.1016/s1360-1385(03)00008-6)
- Piao, S. L., Sitch, S., Ciais, P., Friedlingstein, P., Peylin, P., Wang, X. H., et al. (2013). Evaluation of terrestrial carbon cycle models for their response to climate variability and to CO<sub>2</sub> trends. *Global Change Biology*, *19*(7), 2117–2132. <https://doi.org/10.1111/gcb.12187>
- Poisson, N., Kanakidou, M., & Crutzen, P. J. (2000). Impact of non-methane hydrocarbons on tropospheric chemistry and the oxidizing power of the global troposphere: 3-dimensional modelling results. *Journal of Atmospheric Chemistry*, *36*(2), 157–230. <https://doi.org/10.1023/A:1006300616544>
- Porporato, A., Laio, F., Ridolfi, L., & Rodriguez-Iturbe, I. (2001). Plants in water-controlled ecosystems: Active role in hydrologic processes and response to water stress - III. Vegetation water stress. *Advances in Water Resources*, *24*(7), 725–744. [https://doi.org/10.1016/s0309-1708\(01\)00006-9](https://doi.org/10.1016/s0309-1708(01)00006-9)

- Possell, M., & Hewitt, C. N. (2011). Isoprene emissions from plants are mediated by atmospheric CO<sub>2</sub> concentrations. *Global Change Biology*, 17(4), 1595–1610. <https://doi.org/10.1111/j.1365-2486.2010.02306.x>
- Rienecker, M. M., Suarez, M. J., Gelaro, R., Todling, R., Bacmeister, J., Liu, E., et al. (2011). MERRA: NASA's modern-era retrospective analysis for research and applications. *Journal of Climate*, 24(14), 3624–3648. <https://doi.org/10.1175/jcli-d-11-00015.1>
- Roelofs, G., & Lelieveld, J. (2000). Tropospheric ozone simulation with a chemistry-general circulation model: Influence of higher hydrocarbon chemistry. *Journal of Geophysical Research Atmospheres*, 105(D18), 22697–22712. <https://doi.org/10.1029/2000JD900316>
- Rosenstiel, T. N., Potosnak, M. J., Griffin, K. L., Fall, R., & Monson, R. K. (2003). Increased CO<sub>2</sub> uncouples growth from isoprene emission in an agriforest ecosystem. *Nature*, 421(6920), 256–259. <https://doi.org/10.1038/nature01312>
- Situ, S., Wang, X. M., Guenther, A. B., Zhang, Y. L., Wang, X. M., Huang, M. J., et al. (2014). Uncertainties of isoprene emissions in the MEGAN model estimated for a coniferous and broad-leaved mixed forest in Southern China. *Atmospheric Environment*, 98, 105–110. <https://doi.org/10.1016/j.atmosenv.2014.08.023>
- Sun, Z. H., Niinemets, U., Huve, K., Rasulov, B., & Noe, S. M. (2013). Elevated atmospheric CO<sub>2</sub> concentration leads to increased whole-plant isoprene emission in hybrid aspen (*Populus tremula* × *Populus tremuloides*). *New Phytologist*, 198(3), 788–800. <https://doi.org/10.1111/nph.12200>
- Unger, N. (2014). Human land-use-driven reduction of forest volatiles cools global climate. *Nature Climate Change*, 4(10), 907–910. <https://doi.org/10.1038/nclimate2347>
- Unger, N., Harper, K., Zheng, Y., Kiang, N. Y., Aleinov, I., Arneth, A., et al. (2013). Photosynthesis-dependent isoprene emission from leaf to planet in a global carbon-chemistry-climate model. *Atmospheric Chemistry and Physics*, 13(20), 10243–10269. <https://doi.org/10.5194/acp-13-10243-2013>
- Uppala, S. M., Kallberg, P. W., Simmons, A. J., Andrae, U., Bechtold, V. D., Fiorino, M., et al. (2005). The ERA-40 re-analysis. *Quarterly Journal of the Royal Meteorological Society*, 131(612), 2961–3012. <https://doi.org/10.1256/qj.04.176>
- Weedon, G. P., Balsamo, G., Bellouin, N., Gomes, S., Best, M. J., & Viterbo, P. (2014). The WFDEI meteorological forcing data set: WATCH Forcing Data methodology applied to ERA-Interim reanalysis data. *Water Resources Research*, 50(9), 7505–7514. <https://doi.org/10.1002/2014wr015638>
- Wells, K. C., Millet, D. B., Payne, V. H., Deventer, M. J., Bates, K. H., de Gouw, J. A., et al. (2020). Satellite isoprene retrievals constrain emissions and atmospheric oxidation. *Nature*, 585, 225–233. <https://doi.org/10.1038/s41586-020-2664-3>
- Wilkinson, M. J., Monson, R. K., Trahan, N., Lee, S., Brown, E., Jackson, R. B., et al. (2009). Leaf isoprene emission rate as a function of atmospheric CO<sub>2</sub> concentration. *Global Change Biology*, 15(5), 1189–1200. <https://doi.org/10.1111/j.1365-2486.2008.01803.x>
- Wolfe, G. M., Thornton, J. A., McKay, M., & Goldstein, A. H. (2011). Forest-atmosphere exchange of ozone: Sensitivity to very reactive biogenic VOC emissions and implications for in-canopy photochemistry. *Atmospheric Chemistry and Physics*, 11(15), 7875–7891. <https://doi.org/10.5194/acp-11-7875-2011>
- Wu, S. L., Mickley, L. J., Leibensperger, E. M., Jacob, D. J., Rind, D., & Streets, D. G. (2008). Effects of 2000–2050 global change on ozone air quality in the United States. *Journal of Geophysical Research*, 113(D6), D06302. <https://doi.org/10.1029/2007jd008917>
- Young, P. J., Arneth, A., Schurgers, G., Zeng, G., & Pyle, J. A. (2009). The CO<sub>2</sub> inhibition of terrestrial isoprene emission significantly affects future ozone projections. *Atmospheric Chemistry and Physics*, 9(8), 2793–2803. <https://doi.org/10.5194/acp-9-2793-2009>
- Yue, X., & Unger, N. (2015). The Yale Interactive terrestrial Biosphere model version 1.0: Description, evaluation and implementation into NASA GISS ModelE2. *Geoscientific Model Development*, 8(8), 2399–2417. <https://doi.org/10.5194/gmd-8-2399-2015>
- Yue, X., Unger, N., Keenan, T. F., Zhang, X., & Vogel, C. S. (2015). Probing the past 30-year phenology trend of US deciduous forests. *Biogeosciences*, 12(15), 4693–4709. <https://doi.org/10.5194/bg-12-4693-2015>
- Yue, X., Unger, N., & Zheng, Y. (2015). Distinguishing the drivers of trends in land carbon fluxes and plant volatile emissions over the past 3 decades. *Atmospheric Chemistry and Physics*, 15(20), 11931–11948. <https://doi.org/10.5194/acp-15-11931-2015>
- Zhang, Y., Hu, X. M., Leung, L. R., & Gustafson, W. I. (2008). Impacts of regional climate change on biogenic emissions and air quality. *Journal of Geophysical Research*, 113(D18), D18310. <https://doi.org/10.1029/2008jd009965>
- Zheng, Y., Unger, N., Barkley, M. P., & Yue, X. (2015). Relationships between photosynthesis and formaldehyde as a probe of isoprene emission. *Atmospheric Chemistry and Physics*, 15(15), 8559–8576. <https://doi.org/10.5194/acp-15-8559-2015>

## References From the Supporting Information

- Alves, E. G., Jardine, K., Tota, J., Jardine, A., Yanez-Serrano, A. M., Karl, T., et al. (2016). Seasonality of isoprenoid emissions from a primary rainforest in central Amazonia. *Atmospheric Chemistry and Physics*, 16(6), 3903–3925. <https://doi.org/10.5194/acp-16-3903-2016>
- Alves, E. G., Tota, J., Turnipseed, A., Guenther, A. B., Bustillos, J., Santana, R. A., et al. (2018). Leaf phenology as one important driver of seasonal changes in isoprene emissions in central Amazonia. *Biogeosciences*, 15(13), 4019–4032. <https://doi.org/10.5194/bg-15-4019-2018>
- Bai, J. H. (2015). Estimation of the isoprene emission from the Inner Mongolia grassland. *Atmospheric Pollution Research*, 6(3), 406–414. <https://doi.org/10.5094/apr.2015.045>
- Bai, J. H., Guenther, A., Turnipseed, A., & Duhl, T. (2015). Seasonal and interannual variations in whole-ecosystem isoprene and monoterpene emissions from a temperate mixed forest in Northern China. *Atmospheric Pollution Research*, 6(4), 696–707. <https://doi.org/10.5094/apr.2015.078>
- Bai, J. H., Guenther, A., Turnipseed, A., Duhl, T., Yu, S., & Wang, B. (2016). Seasonal variations in whole-ecosystem BVOC emissions from a subtropical bamboo plantation in China. *Atmospheric Environment*, 124, 12–21. <https://doi.org/10.1016/j.atmosenv.2015.11.008>
- Bai, J. H., Wang, G. C., Ren, L. X., Baker, B., Zimmerman, P., & Liang, B. S. (2003). The emission flux of volatile organic compounds in the Inner Mongolia Grassland. *Huanjing Kexue*, 24(6), 16–22.
- Baker, B., Bai, J. H., Johnson, C., Cai, Z. T., Li, Q. J., Wang, Y. F., et al. (2005). Wet and dry season ecosystem level fluxes of isoprene and monoterpenes from a southeast Asian secondary forest and rubber tree plantation. *Atmospheric Environment*, 39(2), 381–390. <https://doi.org/10.1016/j.atmosenv.2004.07.033>
- Davis, K., Lenschow, D., & Zimmerman, P. (1994). Biogenic nonmethane hydrocarbon emissions estimated from tethered balloon observations. *Journal of Geophysical Research*, 99(D12), 25587–25598. <https://doi.org/10.1029/94JD02009>
- Goldstein, A. H., Goulden, M. L., Munger, J. W., Wofsy, S. C., & Geron, C. D. (1998). Seasonal course of isoprene emissions from a midlatitude deciduous forest. *Journal of Geophysical Research*, 103(D23), 31045–31056. <https://doi.org/10.1029/98jd02708>
- Greenberg, J. P., Guenther, A., Zimmerman, P., Baugh, W., Geron, C., Davis, K., et al. (1999). Tethered balloon measurements of biogenic VOCs in the atmospheric boundary layer. *Atmospheric Environment*, 33(6), 855–867. [https://doi.org/10.1016/s1352-2310\(98\)00302-1](https://doi.org/10.1016/s1352-2310(98)00302-1)

- Greenberg, J. P., Guenther, A. B., Madronich, S., Baugh, W., Ginoux, P., Druilhet, A., et al. (1999). Biogenic volatile organic compound emissions in central Africa during the Experiment for the Regional Sources and Sinks of Oxidants (EXPRESSO) biomass burning season. *Journal of Geophysical Research*, *104*(D23), 30659–30671. <https://doi.org/10.1029/1999jd900475>
- Guenther, A., Archer, S., Greenberg, J., Harley, P., Helmig, D., Klinger, L., et al. (1999). Biogenic hydrocarbon emissions and landcover/climate change in a subtropical savanna. *Physics and Chemistry of the Earth - Part B: Hydrology, Oceans and Atmosphere*, *24*(6), 659–667. [https://doi.org/10.1016/S1464-1909\(99\)00062-3](https://doi.org/10.1016/S1464-1909(99)00062-3)
- Guenther, A., Baugh, W., Davis, K., Hampton, G., Harley, P., Klinger, L., et al. (1996). Isoprene fluxes measured by enclosure, relaxed eddy accumulation, surface layer gradient, mixed layer gradient, and mixed layer mass balance techniques. *Journal of Geophysical Research*, *101*(D13), 18555–18567. <https://doi.org/10.1029/96jd00697>
- Guenther, A., Greenberg, J., Harley, P., Helmig, D., Klinger, L., Vierling, L., et al. (1996). Leaf, branch, stand and landscape scale measurements of volatile organic compound fluxes from US woodlands. *Tree Physiology*, *16*(1–2), 17–24. <https://doi.org/10.1093/treephys/16.1-2.17>
- Guenther, A., Zimmerman, P., Klinger, L., Greenberg, J., Ennis, C., Davis, K., et al. (1996). Estimates of regional natural volatile organic compound fluxes from enclosure and ambient measurements. *Journal of Geophysical Research*, *101*(D1), 1345–1359. <https://doi.org/10.1029/95jd03006>
- Harley, P., Otter, L., Guenther, A., & Greenberg, J. (2003). Micrometeorological and leaf-level measurements of isoprene emissions from a southern African savanna. *Journal of Geophysical Research*, *108*(D13), 8468. <https://doi.org/10.1029/2002jd002592>
- Helmig, D., Balsley, B., Davis, K., Kuck, L. R., Jensen, M., Bognar, J., et al. (1998). Vertical profiling and determination of landscape fluxes of biogenic nonmethane hydrocarbons within the planetary boundary layer in the Peruvian Amazon. *Journal of Geophysical Research*, *103*(D19), 25519–25532. <https://doi.org/10.1029/98jd01023>
- Holst, T., Arneeth, A., Hayward, S., Ekberg, A., Mastepanov, M., Jackowicz-Korczynski, M., et al. (2010). BVOC ecosystem flux measurements at a high latitude wetland site. *Atmospheric Chemistry and Physics*, *10*(4), 1617–1634. <https://doi.org/10.5194/acp-10-1617-2010>
- Isebrands, J. G., Guenther, A. B., Harley, P., Helmig, D., Klinger, L., Vierling, L., et al. (1999). Volatile organic compound emission rates from mixed deciduous and coniferous forests in Northern Wisconsin, USA. *Atmospheric Environment*, *33*(16), 2527–2536. [https://doi.org/10.1016/S1352-2310\(98\)00250-7](https://doi.org/10.1016/S1352-2310(98)00250-7)
- Jensen, N. R., Gruening, C., Goded, I., Muller, M., Hjorth, J., & Wisthaler, A. (2018). Eddy-covariance flux measurements in an Italian deciduous forest using PTR-ToF-MS, PTR-QMS and FIS. *International Journal of Environmental Analytical Chemistry*, *98*(8), 758–788. <https://doi.org/10.1080/03067319.2018.1502758>
- Karl, T., Guenther, A. B., Yokelson, R. J., Greenberg, J., Potosnak, M., Blake, D. R., & Artaxo, P. (2007). The tropical forest and fire emissions experiment: Emission, chemistry, and transport of biogenic volatile organic compounds in the lower atmosphere over Amazonia. *Journal of Geophysical Research*, *112*(D18), D18302. <https://doi.org/10.1029/2007jd008539>
- Karl, T., Potosnak, M., Guenther, A., Clark, D., Walker, J., Herrick, J. D., & Geron, C. (2004). Exchange processes of volatile organic compounds above a tropical rain forest: Implications for modeling tropospheric chemistry above dense vegetation. *Journal of Geophysical Research*, *109*(D18), D18306. <https://doi.org/10.1029/2004jd004738>
- Langford, B., Cash, J., Acton, W. J. F., Valach, A. C., Hewitt, C. N., Fares, S., et al. (2017). Isoprene emission potentials from European oak forests derived from canopy flux measurements: An assessment of uncertainties and inter-algorithm variability. *Biogeosciences*, *14*(23), 5571–5594. <https://doi.org/10.5194/bg-14-5571-2017>
- Langford, B., Misztal, P. K., Nemitz, E., Davison, B., Helfter, C., Pugh, T. A. M., et al. (2010). Fluxes and concentrations of volatile organic compounds from a South-East Asian tropical rainforest. *Atmospheric Chemistry and Physics*, *10*(17), 8391–8412. <https://doi.org/10.5194/acp-10-8391-2010>
- McKinney, K. A., Lee, B. H., Vasta, A., Pho, T. V., & Munger, J. W. (2011). Emissions of isoprenoids and oxygenated biogenic volatile organic compounds from a New England mixed forest. *Atmospheric Chemistry and Physics*, *11*(10), 4807–4831. <https://doi.org/10.5194/acp-11-4807-2011>
- Misztal, P. K., Nemitz, E., Langford, B., Di Marco, C. F., Phillips, G. J., Hewitt, C. N., et al. (2011). Direct ecosystem fluxes of volatile organic compounds from oil palms in South-East Asia. *Atmospheric Chemistry and Physics*, *11*(17), 8995–9017. <https://doi.org/10.5194/acp-11-8995-2011>
- Olofsson, M., Ek-Olausson, B., Jensen, N. O., Langer, S., & Ljungstrom, E. (2005). The flux of isoprene from a willow coppice plantation and the effect on local air quality. *Atmospheric Environment*, *39*(11), 2061–2070. <https://doi.org/10.1016/j.atmosenv.2004.12.015>
- Otter, L. B., Guenther, A., & Greenberg, J. (2002). Seasonal and spatial variations in biogenic hydrocarbon emissions from southern African savannas and woodlands. *Atmospheric Environment*, *36*(26), 4265–4275. [https://doi.org/10.1016/s1352-2310\(02\)00333-3](https://doi.org/10.1016/s1352-2310(02)00333-3)
- Pacifico, F., Harrison, S. P., Jones, C. D., Arneeth, A., Sitch, S., Weedon, G. P., et al. (2011). Evaluation of a photosynthesis-based biogenic isoprene emission scheme in JULES and simulation of isoprene emissions under present-day climate conditions. *Atmospheric Chemistry and Physics*, *11*(9), 4371–4389. <https://doi.org/10.5194/acp-11-4371-2011>
- Park, J. H., Goldstein, A. H., Timkovsky, J., Fares, S., Weber, R., Karlik, J., & Holzinger, R. (2013). Eddy covariance emission and deposition flux measurements using proton transfer reaction - Time of flight - Mass spectrometry (PTR-TOF-MS): Comparison with PTR-MS measured vertical gradients and fluxes. *Atmospheric Chemistry and Physics*, *13*(3), 1439–1456. <https://doi.org/10.5194/acp-13-1439-2013>
- Pattey, E., Desjardins, R. L., Westberg, H., Lamb, B., & Zhu, T. (1999). Measurement of isoprene emissions over a black spruce stand using a tower-based relaxed eddy-accumulation system. *Journal of Applied Meteorology*, *38*(7), 870–877. [https://doi.org/10.1175/1520-0450\(1999\)038<0870:Moieoa>2.0.CO;2](https://doi.org/10.1175/1520-0450(1999)038<0870:Moieoa>2.0.CO;2)
- Pressley, S., Lamb, B., Westberg, H., Flaherty, J., Chen, J., & Vogel, C. (2005). Long-term isoprene flux measurements above a northern hardwood forest. *Journal of Geophysical Research*, *110*(D7), D07301. <https://doi.org/10.1029/2004jd005523>
- Rhew, R. C., Deventer, M. J., Turnipseed, A. A., Warneke, C., Ortega, J., Shen, S., et al. (2017). Ethene, propene, butene and isoprene emissions from a ponderosa pine forest measured by relaxed eddy accumulation. *Atmospheric Chemistry and Physics*, *17*(21), 13417–13438. <https://doi.org/10.5194/acp-17-13417-2017>
- Rinne, J., Guenther, A., Greenberg, J., & Harley, P. (2002). Isoprene and monoterpene fluxes measured above Amazonian rainforest and their dependence on light and temperature. *Atmospheric Environment*, *36*(14), 2421–2426. [https://doi.org/10.1016/s1352-2310\(01\)00523-4](https://doi.org/10.1016/s1352-2310(01)00523-4)
- Rinne, J., Tuovinen, J., Laurila, T., Hakola, H., Aurela, M., & Hypén, H. (2000). Measurements of hydrocarbon fluxes by a gradient method above a northern boreal forest. *Agricultural and Forest Meteorology*, *102*, 25–37. [https://doi.org/10.1016/S0168-1923\(00\)00088-5](https://doi.org/10.1016/S0168-1923(00)00088-5)
- Saito, T., Yokouchi, Y., Kosugi, Y., Tani, M., Philip, E., & Okuda, T. (2008). Methyl chloride and isoprene emissions from tropical rain forest in Southeast Asia. *Geophysical Research Letters*, *35*(19), L19812. <https://doi.org/10.1029/2008gl035241>

- Serca, D., Guenther, A., Klinger, L., Vierling, L., Harley, P., Druilhet, A., et al. (2001). EXPRESSO flux measurements at upland and lowland Congo tropical forest site. *Tellus Series B Chemical and Physical Meteorology*, 53(3), 220–234. <https://doi.org/10.1034/j.1600-0889.2001.01237.x>
- Spirig, C., Guenther, A., Greenberg, J. P., Calanca, P., & Tarvainen, V. (2004). Tethered balloon measurements of biogenic volatile organic compounds at a Boreal forest site. *Atmospheric Chemistry and Physics*, 4, 215–229. <https://doi.org/10.5194/acp-4-215-2004>
- Spirig, C., Neftel, A., Ammann, C., Dommen, J., Grabmer, W., Thielmann, A., et al. (2005). Eddy covariance flux measurements of biogenic VOCs during ECHO 2003 using proton transfer reaction mass spectrometry. *Atmospheric Chemistry and Physics*, 5, 465–481. <https://doi.org/10.5194/acp-5-465-2005>
- Steinbrecher, R., Klauer, M., Hauff, K., Stockwell, W. R., Jaeschke, W., Dietrich, T., & Herbert, F. (2000). Biogenic and anthropogenic fluxes of non-methane hydrocarbons over an urban-impacted forest, Frankfurter Stadtwald, Germany. *Atmospheric Environment*, 34(22), 3779–3788. [https://doi.org/10.1016/s1352-2310\(99\)00518-x](https://doi.org/10.1016/s1352-2310(99)00518-x)
- Stoy, P. C., Trowbridge, A. M., Siqueira, M. B., Freire, L. S., Phillips, R. P., Jacobs, L., et al. (2021). Vapor pressure deficit helps explain biogenic volatile organic compound fluxes from the forest floor and canopy of a temperate deciduous forest. *Oecologia*, <https://doi.org/10.1007/s00442-021-04891-1>
- Zheng, Y. Q., Unger, N., Tadic, J. M., Seco, R., Guenther, A. B., Barkley, M. P., et al. (2017). Drought impacts on photosynthesis, isoprene emission and atmospheric formaldehyde in a mid-latitude forest. *Atmospheric Environment*, 167, 190–201. <https://doi.org/10.1016/j.atmosenv.2017.08.017>